journal

J. Am. Ceram. Soc., **83** [10] 2409–16 (2000)

Solid Freeform Fabrication of Aqueous Alumina–Poly(vinyl alcohol) Gelcasting Suspensions

Sherry L. Morissette*,† and Jennifer A. Lewis*

Department of Materials Science and Engineering, University of Illinois, Urbana, Illinois 61801

Joseph Cesarano III,* Duane B. Dimos,* and Tom Baer

Direct Fabrication Department, Sandia National Laboratories, Albuquerque, New Mexico 87185

Solid freeform fabrication of aqueous alumina–poly(vinyl alcohol) (Al_2O_3–PVA) gel-casting suspensions was conducted using a computer-controlled extrusion apparatus fitted with a two-nozzle delivery system. The impact of casting parameters on the shear rate profiles experienced during deposition was evaluated via conventional flow analysis and computer simulations. In addition, the influence of these parameters on line resolution/uniformity, printability, and as-cast component properties was studied using laser profilometry, optical microscopy, and scanning electron microscopy. Continuous printablity was achieved for tip diameters ranging from 0.254 to 1.370 mm for all mixing rates and suspension compositions studied. Printed lines were uniform with good edge definition, and line dimensions were independent of mixing rate for these process conditions. The Al_2O_3 volume fraction ($\phi_{Al_2O_3}$) in the as-deposited layers depended on casting conditions and cross-linking agent concentration, where ($\phi_{Al_2O_3}$ increased with decreased tip diameter and increased cross-linking agent concentration. The free-formed Al_2O_3 components exhibited uniform particle packing, with minimal macrodefects (e.g., slumping or staircasing) and no discernable microdefects (e.g., bubbles or cracking).

I. Introduction

THE continual drive toward agile, facile methods for producing near-net-shaped advanced ceramic components has led to a revolutionary class of forming techniques known as solid freeform fabrication (SFF). Such techniques use computer-controlled robotics to build three-dimensional components in a layer-by-layer fashion. The advantages of SFF over conventional fabrication methods include spatially tailored composition, greater process control and flexibility, lower tooling costs, and improved performance/reliability. To date, several SFF techniques, including stereolithography (SLA),[1–6] fused deposition of ceramics (FDC),[7–11] laminated object manufacturing (LOM),[12] computer-aided manufacturing of laminated engineering materials (CAM-LEM),[13] three-dimensional printing (3DP™),[14–18] and robocasting,[19,20] have been developed. However, many of these approaches rely on feedstocks that contain 40–70 vol% organic species, which results in debinding issues that limit feasible component sizes to ~1 mm or less thickness.

Robocasting[19,20] is a slurry deposition technique capable of producing large-scale, near-net-shaped components that utilizes feedstocks of negligible organic content (<1 vol%). In robocasting, pseudoplastic ceramic suspensions (solids volume fraction (ϕ_{solids}) ~0.50) are deposited onto a substrate in a precise pattern. On minimal drying, the as-deposited suspension undergoes a liquid-to-solid transition that freezes-in the structure of the patterned element. Current challenges to this approach involve controlling the macroscopic shape evolution of the as-deposited components. Slumping, which results from insufficient drying in high-aspect-ratio multilayer components, and considerable staircasing in component walls have been observed. Hence, there is a need to develop new feedstock materials with low organic content, such as gelcasting suspensions, to improve the mechanical strength of the deposited layers and, thereby, overcome these limitations.

Gelcasting[21–28] is a bulk fabrication technique for producing near-net-shaped ceramic components. Gelcasting uses systems of low organic content (≤5 vol%) that undergo gelation via either polymerization of monomeric species[21–26] or cross-linking of existing polymeric species in solution.[27–30] The resulting polymeric network provides shape retention without drying and serves as the binder phase for the as-cast component, imparting sufficient strength for green machining. Morissette and Lewis[27] have investigated the chemorheological properties of aqueous alumina–poly(vinyl alcohol) (Al_2O_3–PVA) gelcasting suspensions and have found that the gelation behavior of this system can be tailored by varying the suspension composition (i.e., ϕ_{solids}, PVA content, and cross-linking agent concentration) as well as the processing temperature. Surprisingly, little attention has been given to the use of such chemically reactive (gelling) systems in current SFF fabrication routes.[31–33]

Here, SFF of aqueous Al_2O_3–PVA gelcasting suspensions was conducted using a computer-controlled extrusion apparatus fitted with a two-nozzle delivery system. The influence of suspension chemorheology and processing parameters (e.g., mixing rate and tip diameter) on the SFF forming behavior was investigated, where the macroscopic shape evolution of printed lines and the properties of as-cast components—including bulk density, microstructure, and wall/layer uniformity—were studied using laser profilometry, as well as optical and scanning electron microscopies. The shear-rate profiles during free-forming were estimated using conventional flow analysis and computer simulations. This allowed processing conditions to be correlated with suspension rheology and deposition behavior. As-cast SFF-derived components exhibited uniform particle packing comparable to bulk gelcast components and had minimal macrodefects (e.g., slumping or staircasing) and no detectable microdefects (e.g., bubbles or cracking). Thus, use of gelcasting suspensions as feedstock materials provides a novel approach for tailoring deposition behavior and, hence, component properties of SFF-derived, advanced ceramic components.

V. A. Hackley—contributing editor

Manuscript No. 188920. Received November 29, 1999; approved March 29, 2000.
Supported by the National Science Foundation under Grant No. DMR94–53446 and the U.S. Department of Energy under Contract No. DE-AC04–94AL8500.
Sandia is a multiprogram laboratory operated by Sandia Corporation, a Lockheed Martin Company, for the U.S. Department of Energy.
*Member, American Ceramic Society.
†Now with the Materials Processing Center, Massachusetts Institute of Technology, Cambridge, MA 02139.

II. Experimental Procedure

(1) Materials System

Al_2O_3 powder (AKP-30, Sumitomo Chemical Co., New York), with a specific surface area of 8.0 m^2/g, as determined via BET analysis (ASAP, Model 2400, Micrometrics, Inc., Norcross, GA), and a mean particle size of 0.4 μm, as determined by particle-size analysis (Model APA-700, Horiba, Kyoto, Japan), served as the ceramic phase. Darvan C (R. T. Vanderbilt Co., Inc., Norwalk, CT), a 25 wt% aqueous solution of ammonium polymethacrylate (APMA), was used as the dispersant.[34] Partially hydrolyzed PVA (405S, Kuraray International Corp., New York), with a degree of hydrolysis of 80.8 mol% and an average molecular weight of 28 700 g/mol, was utilized as the polymeric additive.[35] Tyzor TE (DuPont Chemicals, Deepwater, NJ) was selected as the cross-linking agent, because it has been shown to react with PVA to form a gel under appropriate conditions.[27,35–37] Tyzor TE contains 8.3 wt% titanium, as confirmed via thermogravimetric analysis (TGA; Model High Res-2950, TA Instruments, Newark, DE), and consists of a 25 wt% solution (in isopropyl alcohol) of various oganotitanate chelates.[38] The proposed cross-linking reaction sequence had been discussed previously.[27,35–37] A short-chain alcohol, 1-octanol (Aldrich Chemical Co., Milwaukee, WI), was utilized as a defoamer in this work to minimize mircodefects associated with bubble formation.

(2) Suspension Preparation

Feedstock suspensions were prepared by adding an appropriate amount of Al_2O_3 powder to an aqueous solution containing 0.012 g of Darvan C/(g of Al_2O_3). Suspensions were ultrasonicated (Model 550 Sonic Dismembrator, Fisher Scientific, Itasca, IL) at 1 s pulsed intervals for 150 s, and subsequently magnetically stirred for 12 h to allow dispersant adsorption onto Al_2O_3 powder surfaces. An appropriate amount of PVA stock solution, prepared by dissolving PVA in deionized water under ambient conditions, was added to each suspension. The pH of each suspension was adjusted to 8.5 ± 0.1 using HNO_3 or NH_4OH. Suspensions were defoamed by addition of 0.25% 1-octanol by volume of solution and mixed for 2 h using a slow roll mill before casting. These suspensions were prepared with a reduced solvent content to account for the volume of cross-linking agent to be added, such that the effective ϕ_{solids} ranged from 0.450 to 0.468, corresponding to cross-linking agent concentrations of $0–6.30 \times 10^{-3}$ g of titanium/(mL of solution).

(3) Suspension Characterization

Representative casting suspensions ($\phi_{Al_2O_3} = 0.45$, $\phi_{PVA}^{soln} = 0.05$) were characterized prior to cross-linking agent addition using a controlled stress (CS) rheometer (Model CS-10, Bohlin Instruments, Cranbury, NJ) in stress viscometry mode, where the apparent suspension viscosity (η_{app}^{susp}) was measured as a function of shear rate ($\dot{\gamma}$) under isothermal conditions ($T = 15.0° \pm 0.1°C$). The CS rheometer was fitted with a concentric cylinder (Model C25, Bohlim Instruments) geometry in which measurements were made over a stress range of 0.025–240 Pa in ascending order. A specially designed solvent trap filled with deionized water was used to minimize solvent loss during measurement. In addition, a layer of silicone oil (Brookfield Engineering Laboratory, Inc., Stoughton, MA) ($\eta = 1000$ cP) was gently placed on the suspension surface to further minimize solvent evaporation over extended measurement periods. No interaction between the samples and silicone oil was observed.

(4) Component Fabrication

Ceramic components were bulk cast or free formed using a slurry deposition technique.[19,20,33] Bulk samples were prepared by separately equilibrating the suspension and cross-linking agent at 5.0° ± 0.1°C, then adding an appropriate amount of the organotitanate cross-linking agent to the suspension, homogenizing the components, and pouring the mixture into polyethylene molds coated with a non-silicone release agent (Moldwiz AZ, Axel Plastics Research Laboratories, Inc., Woodside, NY). Samples were gelled *in situ*, removed from the molds, and dried in a series of controlled humidity chambers.[39]

Free-formed components were cast using a computer-controlled extrusion apparatus fitted with a two-nozzle delivery system (Robocasting apparatus, Sandia National Laboratories, Albuquerque, NM), as illustrated schematically in Fig. 1. The ceramic suspension and cross-linking agent (Tyzor TE) solution were loaded into separate 30 mL polyethylene syringes. The syringes were clamped into the SFF apparatus housings, each of which was fitted with a cooling coil that chilled the gelcasting components to 15.0° ± 0.02°C to minimize gelation in the mixing chamber. The ceramic suspension and cross-linking agent were pumped into the mixing chamber at controlled ratios, homogenized using a paddle-type mixer, extruded from the tip orifice, and deposited in a precise pattern onto a moving ***X–Y*** table via computer-aided design (CAD) instruction. Three-dimensional components (1.0 cm × 1.0 cm × 0.5 cm) were constructed using a layer-by-layer build sequence. The ***X–Y*** table was heated to 30.0° ± 1.0°C using resistance heaters to enhance gelation kinetics in the deposited layers.

Single-line prints and three-dimensional components were cast under different conditions, including cross-linking concentrations of [Ti] = 0.0, 3.04×10^{-3}, and 6.30×10^{-3} g of titanium/(mL of solution); mixing rates (R_{mix}) of 0–300 rpm; and tip diameters (d_t) of 0.254–1.37 mm. The printability of the system was determined by depositing a single line in a serpentine pattern. If this pattern could be printed continuously for at least 10 min, then the system was defined as printable. Samples were dried either in air under ambient conditions or in a controlled humidity environment.[39]

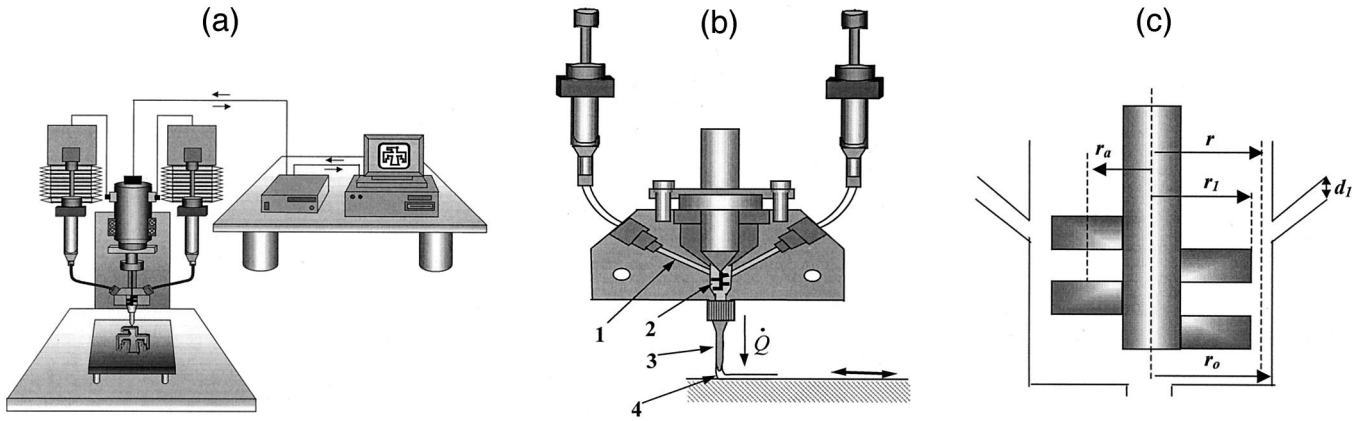

Fig. 1. Schematic illustrations of (a) robocasting apparatus, (b) two-nozzle delivery system showing four shear zones in the mixing chamber ((1) pumping from the syringe ($\dot{\gamma}_p$), (2) mixing via paddle mixer ($\dot{\gamma}_{mix}$), (3) extrusion from the tip ($\dot{\gamma}_{ext}$), and (4) deposition onto the moving ***X–Y*** table ($\dot{\gamma}_{dep}$)), and (c) paddle design, where $r = 1.651$ mm, $r_a = 0.89$ mm, $r_1 = 1.59$ mm, $r_0 = 1.72$ mm, and $d_1 = 1.52$ mm.

(5) Component Properties

The effects of processing parameters on the properties of as-cast bulk- and SFF-derived components were evaluated using a variety of techniques. Line and layer thickness uniformity of dried, as-cast bodies was characterized using scanning laser profilometry (Robocasting apparatus, Sandia National Laboratories) and optical microscopy (Model Stemi SV11, Carl Zeiss, Inc., Thornwood, NY). The density of as-cast components was measured via geometrical methods. Scanning electron microscopy (SEM) was used to analyze component microstructure, including defect/void population and particle packing.

III. Results and Discussion

(1) Modeling of Flow Behavior during SFF Fabrication

The free-forming process generates various shear environments depending on the stage of the deposition sequence. This sequence can be divided into four zones, each of which is defined by a characteristic shear-rate ($\dot{\gamma}$) regime, as illustrated in Fig. 1(b), including (1) pumping from the syringe ($\dot{\gamma}_p$), (2) mixing via the paddle mixer ($\dot{\gamma}_{mix}$), (3) extrusion from the tip ($\dot{\gamma}_{ext}$), and (4) deposition onto the moving ***X–Y*** table ($\dot{\gamma}_{dep}$). The shear-rate ranges for each of these zones were estimated to identify the boundary shear-rate conditions for varying process conditions. These shear-rate ranges were used to correlate the effects of processing parameters on the rheological properties and, hence, deposition behavior of the casting suspensions during free forming. The methods used to estimate the shear-rate ranges associated with each zone are outlined below.

(A) Zone 1—Syringe Transfer: The syringe plunger acts as a piston that forces the suspension from the syringe into the mixing chamber. Flow of the suspension is most restricted at the mixing chamber inlet, which has a diameter of 1.52 mm. A gradient in the shear-rate profile is expected for flow through this cylindrical channel, where the maximum shear rate ($\dot{\gamma}_{max}$) occurs near the vessel wall and is given by[40,41]

$$\dot{\gamma}_{max} = \frac{4\dot{Q}}{\pi r^3} \tag{1}$$

where $\dot{Q}$ is the volume flow rate and r the radius of the inlet channel. Thus, $\dot{\gamma}_{max}$ varies directly with $\dot{Q}$ according to $\dot{\gamma}_{max} = 2.9\dot{Q}$. The inlet $\dot{Q}$ depends on the table speed (s_t), tip diameter (d_t), and layer thickness (t_l), as given by $\dot{Q} = s_t d_t t_l$. For typical inlet $\dot{Q}$ rates of 0–0.02 mL/s, $\dot{\gamma}_{max}$ at the inlet wall ranges from 0 to 60 s^{-1}.

(B) Zone 2—Mixing Chamber: The mixing apparatus, which consists of a double-edged, comb-shaped paddle and a cylindrical chamber, as illustrated in Fig. 1(c), is modeled using a coaxial cylinder approximation. The radius of the inner cylinder, i.e., the paddle, varies from its maximum value of $r_1 = 1.59$ mm to an average value of $r_a = 0.89$ mm (refer to Fig. 1(c)). The radius of the mixing chamber is $r_0 = 1.72$ mm. $\dot{\gamma}_{mix}$ is evaluated at a constant radius, i.e., $r = 1.651$ mm, according to[42]

$$\dot{\gamma}_{mix} = \frac{4\pi f r_1^2 r_0^2}{r^2(r_0^2 - r_1^2)} \tag{2}$$

where f is the frequency of rotation, r_1 the radius of the paddle, r_0 the radius of mixing chamber, and $r = (r_1 + r_0)/2$. $\dot{\gamma}_{mix}$ is plotted as a function of R_{mix} for the maximum and average paddle radii in Fig. 2, where $\dot{\gamma}_{mix}$ for typical deposition conditions ranges from 10 to 400 s^{-1}.

(C) Zone 3—Extrusion from Tip: Extrusion of the suspension from the tip induces shear behavior analogous to that calculated for flow through the mixing chamber inlet (zone 1), where $\dot{\gamma}_{max}$ at the inlet walls is given by Eq. (1) for $\dot{Q}$ and R. $\dot{Q} = s_t d_t t_l$ is calculated for varying s_t and t_l for $d_t = 0.254$ mm and $d_t = 1.37$ mm, the minimum and maximum tip diameters used, respectively. These data are compiled into contour maps of maximum $\dot{\gamma}_{ext}$ as a function of s_t and t_l, as illustrated in Figs. 3(a) and (b). $\dot{\gamma}_{ext}$ values of 0.1–400 s^{-1} are expected.

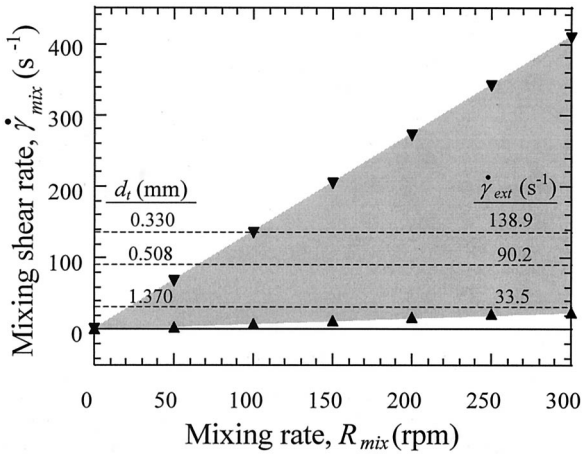

Fig. 2. Mixing shear rate ($\dot{\gamma}_{mix}$) as a function of mixing rate (R_{mix}) ((- - -) maximum extrusion shear rate ($\dot{\gamma}_{ext}$) for the given tip diameter). (Shear rates were calculated using concentric cylinder estimation.)

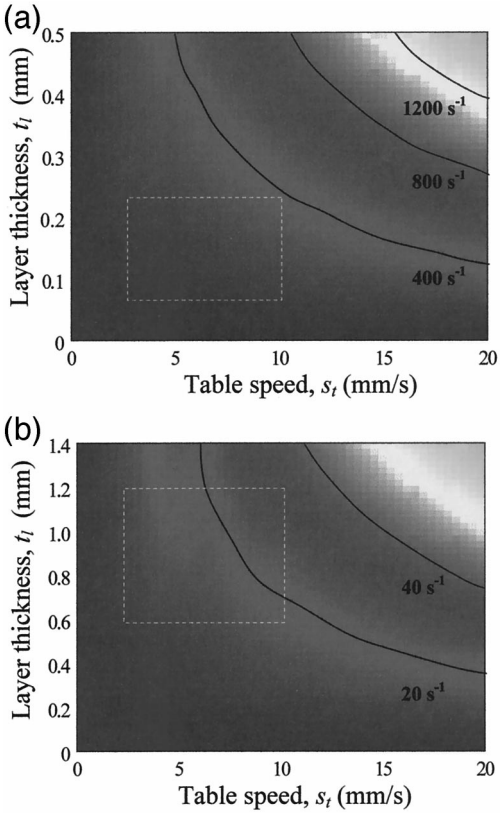

Fig. 3. Contour plots of maximum shear rate ($\dot{\gamma}_{ext}$) as a function of table speed (s_t) and layer thickness (t_l) for tip diameters (d_t) of (a) 0.254 and (b) 1.37 mm (dashed regions highlight typical deposition conditions).

(D) Zone 4—Deposition onto Moving Table: Patterning of the suspension onto the moving **X**–**Y** table results in shear stress at the suspension/table interface. The shear rate range at the contact interface is simulated using GOMA 2.0 for typical deposition conditions. GOMA[43] is a full-Newton finite-element program for analysis of manufacturing flows and related processes. GOMA uses a fully implicit, pseudosolid, unstructured mesh deformation algorithm that allows all boundaries and interfaces to be treated as free (position unknown) or moving (position unknown or prescribed, but variable). For Newtonian fluids, an Arbitrary-Lagrangian-Eulerian (ALE) formulation allows the boundaries to respond to constraint equations or distinguishing conditions.[43] These distinguishing conditions define the location of all boundaries and interfaces, providing the necessary mathematical closure of the

system of equations governing the free-boundary problem, i.e., the distinguishing conditions correlate the mesh deformation behavior and the physics of interest.[43]

GOMA has been used to model numerous processes relevant to ceramics processing, including coating operations, axisymmetric extrusion, simple mold filling and drying, and shrinking of deformable porous media.[43] Here, the deposition behavior of ceramic suspensions onto a moving substrate has been modeled by solving the Navier–Stokes equation, given by[40]

$$\frac{\partial V}{\partial t} + (V\cdot\nabla)V = -\frac{1}{p}\nabla_p - \nabla_g + \nu\nabla^2 V \qquad (3)$$

where V is the velocity, ρ the density, ∇_p the momentum gradient, ∇_g the gravity gradient, and ∇ the vector operator *del* defined as $\mathbf{V}() = \mathbf{i}\partial()/\partial x + \mathbf{j}\partial()/\partial y + \mathbf{k}\partial()/\partial z$. This solution, however, is applicable only to Newtonian fluids. Therefore, simulations were performed for upper- and lower-bounding apparent viscosities (i.e., 1 and 100 Pa·s) to determine the significance of viscosity effects on the maximum shear rates attained. The results of these simulations are shown in Figs. 4(a) and (b), where the calculated $\dot{\gamma}$ values for $d_t = 0.254$ mm, $s_t = 5$ mm/s, $t_l = 0.227$ mm ($t_l = 0.9d_t$), and $\dot{Q} = 0.00025$ mL/s are illustrated for suspensions with Newtonian viscosities of 1 and 100 Pa·s, respectively. In both cases, $\dot{\gamma}_{max} = 250\ s^{-1}$ occurs at the initial contact interface between the suspension and table, where $\dot{\gamma}$ decreases rapidly to zero at short distances beyond this first contact interface. The shear rates at the contact point are relatively high; however, the volume of suspension they influence is small. Thus, the impact of shear due to deposition (zone 4) is likely negligible compared with the shear experienced during mixing (zone 2) and extrusion from the tip (zone 3). No observable differences in the shear rate profiles have been found with varying suspension viscosity, suggesting the Navier–Stokes solution is satisfactory over the range of suspension viscosities utilized.

The influence of d_t on the shear rate profile during deposition is shown in Figs. 4(a) and (c) for $d_t = 0.254$ mm and $d_t = 1.370$ mm at constant $s_t = 5$ mm/s, $t_l = 0.227$ mm ($\sim 0.9d_t$), and $\eta = 100$ Pa·s). $\dot{\gamma}_{max}$ at the suspension/table interface decreased 100 s^{-1} as d_t increased from 0.254 to 1.370 mm. Because $\dot{Q}$ was directly proportional to d_t, (i.e., $\dot{Q} \propto d_t^2$), the observed reduction in $\dot{\gamma}$ at the contact point likely resulted from the increase in contact area, where the flow was distributed over a larger area. However, this behavior also could be attributed to complicated flow behavior that resulted in flow acceleration and, thus, greater flow velocities.[43]

The impact of s_t on $\dot{\gamma}$ values during deposition is illustrated in Figs. 4(d) and (a) for suspensions ($\eta = 100$ Pa·s) cast at a constant $d_t = 0.254$ mm, $t_l = 0.227$ mm ($\sim 0.9d_t$), and $\dot{Q} = 0.00025$ mL/s at $s_t = 2.5$ mm/s and s_t 5.0 mm/s, respectively. $\dot{\gamma}$ at the contact

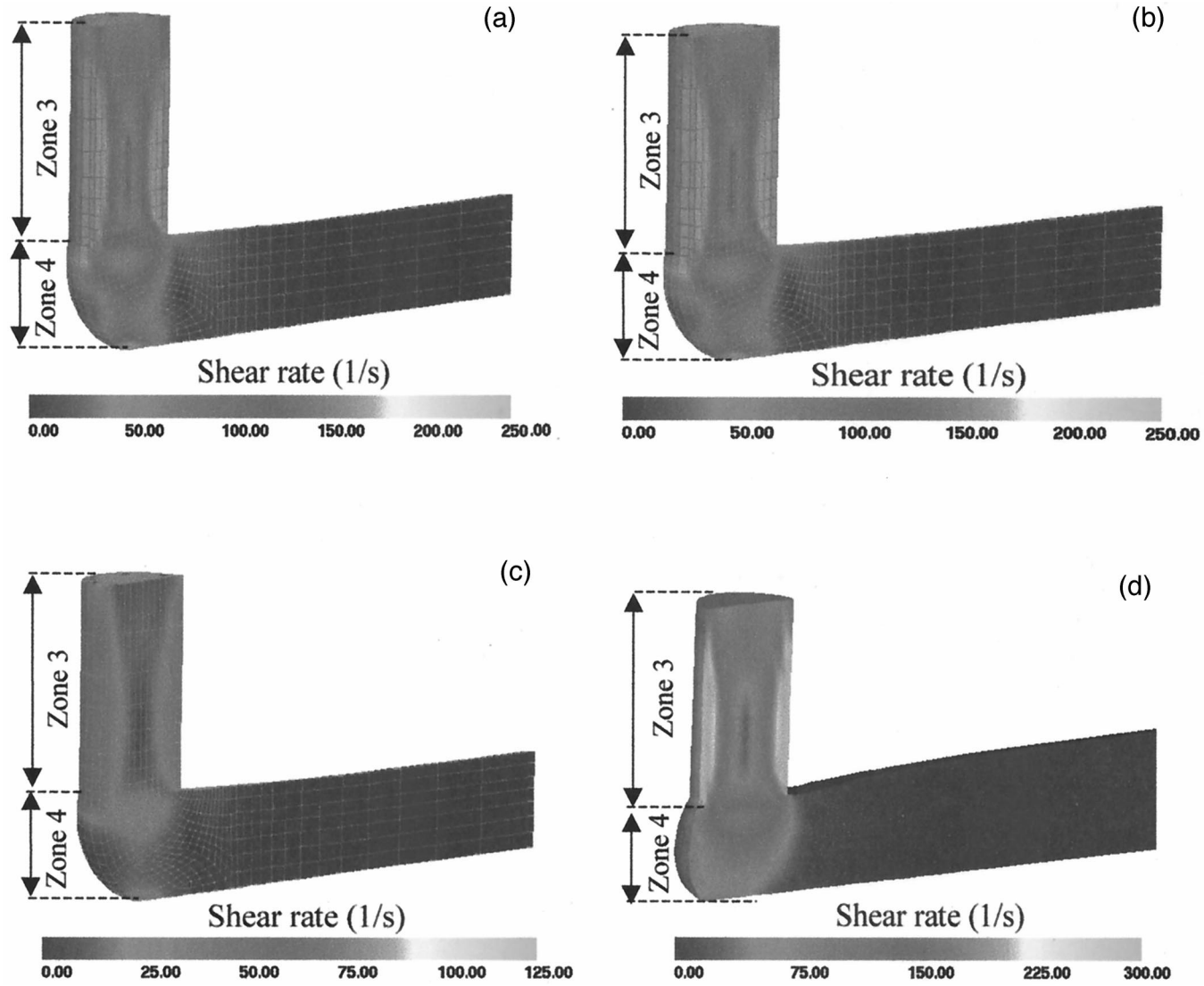

Fig. 4. Calculated shear rate ($\dot{\gamma}$) for varying suspension viscosity (η), tip diameter (d_t), and table speed (s_t): (a) $\eta = 1$ Pa·s, $d_t = 0.254$ mm, $s_t = 5$ mm/s; (b) $\eta = 100$ Pa·s, $d_t = 0.254$ mm, $s_t = 5$ mm/s; (c) $\eta = 100$ Pa·s, $d_t = 1.370$ mm, $s_t = 5$ mm/s; and (d) $\eta = 100$ Pa·s, $d_t = 0.254$ mm, $s_t = 2.5$ mm/s ($t_l = 0.227$ mm ($t_l = 0.9d_t$)).

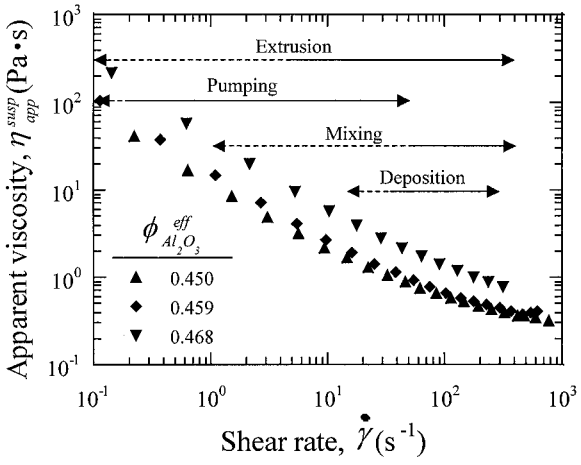

Fig. 5. Apparent viscosity (η_{app}) as a function of shear rate ($\dot{\gamma}$) for representative casting suspensions with varying effective solids volume fractions ($\phi^{eff}_{Al_2O_3}$) before cross-linking agent addition measured at 15.0° ± 0.1°C ((- - -) possible range and (—) working range).

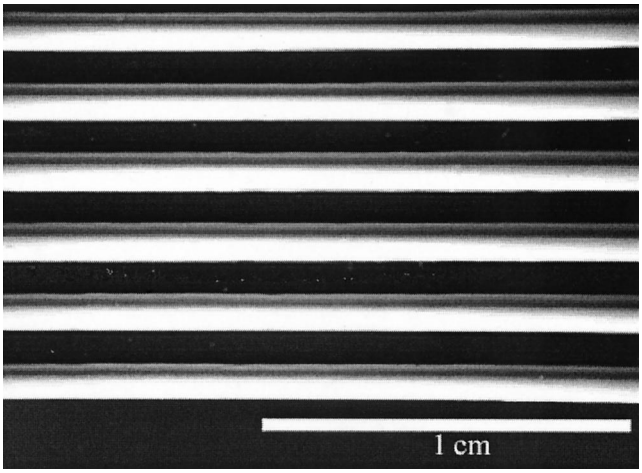

Fig. 6. Optical photomicrograph of the top view of lines cast from a representative suspension ($\phi_{Al_2O_3}$ = 0.45, ϕ_{PVA} = 0.275, [Ti] = 3.041 × 10^{-3} g of titanium/(mL of solution)) printed at a constant tip diameter of 0.330 mm at R_{mix} = 50 rpm.

interface decreased with decreased s_t, as evidenced by the $\dot{\gamma}_{max}$, which increased by ~100 s^{-1} when s_t was increased by a factor of 2. A decrease in s_t for a given $\dot{Q}$ = 0.00025 mL/s led to the formation of a suspension bead that was larger than the outer tip diameter (indicative of excess flow).

The above calculations show that the processing conditions have a significant impact on the shear rate ranges expected during SFF fabrication, where the greatest shear rates occur during the mixing, extrusion, and deposition processes. However, because the shear induced during deposition influences a relatively small volume of fluid, it is likely that its contribution is negligible relative to the mixing and extrusion zones. A comparison of the characteristic shear rates for these processes is provided in Fig. 2 for s_t = 5 mm/s as used in the fabrication of SFF samples in this work. $\dot{\gamma}_{ext}$ exceeds the average $\dot{\gamma}_{mix}$ in all cases, suggesting extrusion-controlled deposition behavior when $\dot{\gamma}_{mix}$ is assigned its average value. However, as R_{mix} increases, $\dot{\gamma}_{mix} > \dot{\gamma}_{ext}$. This crossover behavior occurs at a given mixing rate that depends on d_t. For example, at d_t = 0.330 mm, the crossover occurs at 100 rpm as the maximum $\dot{\gamma}_{mix}$ exceeds the $\dot{\gamma}_{ext}$. In the following sections, the influence of processing conditions and the corresponding shear rate conditions on suspension rheology and the resulting deposition behavior are discussed.

(2) Rheological Behavior of Casting Suspensions

η^{susp}_{app} as a function of $\dot{\gamma}$ for feedstock suspensions (i.e., suspensions without cross-linking agent addition) is shown in Fig. 5. All suspensions exhibited moderate shear-thinning behavior, where η^{susp}_{app} decreased ~2 orders of magnitude over the process shear rate range denoted in Fig. 5. As expected, η^{susp}_{app} increased with increased effective solids volume fraction ($\phi^{eff}_{Al_2O3}$). The estimated shear rate ranges for each step of the casting process are highlighted in Fig. 5, where the possible shear rate ranges are indicated by dashed lines and the actual process shear rates are represented by solid lines. Under typical deposition conditions, feedstock suspensions had η^{susp}_{app} ranging from 0.1 to 100 Pa·s.

(3) Effects of Processing Parameters on Deposition Behavior

Continuous printing was achieved at d_t = 0.254 mm to d_t = 1.370 mm for all R_{mix} = 5 rpm to R_{mix} = 300 rpm and all suspension compositions (i.e., $\phi_{Al_2O_3}$ = 0.45, ϕPVA = 0.275, [Ti] = 0–6.30 × 10^{-3} g of titanium/(mL of solution)) studied. The minimum d_t for continuous printing was 0.203 mm. Constant flow from the nozzle was achieved at smaller tip diameters (i.e., 0.102 mm); however, drying at the tip prevented uninterrupted printing.

Printed lines were uniform with good edge definition for all deposition conditions, as illustrated in Fig. 6 for representative lines printed at a constant d_t = 0.330 mm and R_{mix} = 50 rpm. Laser profilometry scans of dried lines printed at varying R_{mix} are shown in Fig. 7, where line height (h_l) is plotted as a function of cross-sectional distance (X) for a representative feedstock suspension $\phi_{Al_2O_3}$ = 0.45, ϕPVA = 0.275, [Ti] = 3.041 × 10^{-3} g of titanium/(mL of solution)) printed at a constant d_t = 0.33 mm and at varying R_{mix} = 0 to R_{mix} = 300 rpm. R_{mix} did not have a significant effect on line uniformity, as illustrated in Fig. 6, or on the line dimensions (i.e., average h_l and width (w_l)), as illustrated in Figs. 8(a) and (b), where the average dried h_l and w_l, respectively, are plotted as a function of R_{mix}. Such behavior was expected when $\dot{\gamma}_{ext} > \dot{\gamma}_{mix}$. This condition was observed only when $\dot{\gamma}_{mix}$ equaled its average value or less (refer to Fig. 2). The average dried line width (w_l = 0.84 ± 0.02 mm) was ~1.3 times the outer diameter of the tip (d_t = 0.64 mm) and the average dried line height (h_l = 0.20 ± 0.01 mm) was ~82% of the initial layer thickness (l_t = 0.245 mm). The expanded line widths observed may have resulted from either spreading of the suspension after deposition given its shear-thinning behavior or overpumping of the suspension where the suspension bead exceeded the tip edge (refer to Fig. 4(d)).

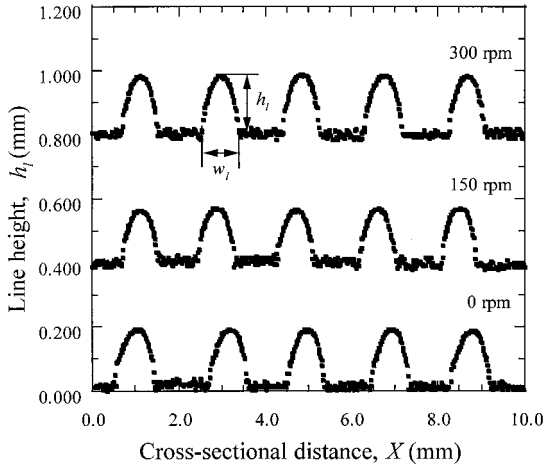

Fig. 7. Laser profilometry scans showing dried line height (h_l) and width (w_l) as a function of cross-sectional distance for lines cast printed at a constant tip diameter.

(4) Properties of As-Cast SFF-Derived Components

(A) Density of As-Cast SFF Bodies: The $\phi_{Al_2O_3}$ of as-cast SSF-derived components fabricated at varying R_{mix} and d_t are shown in Figs. 9(a) and (b) for [Ti] = 0.0 g of titanium/(mL of solution) and [Ti] = 6.30×10^{-3} g of titanium/(mL of solution), respectively. $\phi_{Al_2O_3}$ of all gelcasting formulations exhibited a d_t dependence, where $\phi_{Al_2O_3}$ increased with decreased d_t. These results were expected at low R_{mix} (i.e., $R_{mix} < 25$ rpm), because this processing regime was extrusion controlled, i.e., $\dot{\gamma}_{ext} > \dot{\gamma}_{mix}$ for all d_t. In this regime, $\dot{\gamma}_{ext}$ increased with decreased d_t, resulting in lower suspension viscosity and improved particle packing. d_t effects also were observed at higher $\dot{\gamma}_{mix}$, suggesting that $\dot{\gamma}_{ext} > \dot{\gamma}_{mix}$ for all processing conditions (i.e., $\dot{\gamma}_{mix}$ is equal to or less than its average value). Alternatively, if $\dot{\gamma}_{mix}$ is greater than its average value, the origin of this trend is unclear.

Samples cast from suspensions containing 6.30×10^{-3} g of titanium/(mL of solution) showed a moderate dependence on R_{mix}, where $\phi_{Al_2O_3}$ decreased with increased R_{mix} for $R_{mix} > 50$ rpm for all d_t. Although the origin of this dependence is unclear, only slight variations in ϕ_{solids} were observed. $\phi_{Al_2O_3}$ of SFF-derived components was comparable to SFF samples devoid of cross-linking agent additions, as well as bulk cast samples with [Ti] = 0.0 g of titanium/(mL of solution), ($\phi_{Al_2O_3} = 0.501$) and without [Ti] = 3.04×10^{-3} g of titanium/(mL of solution) ($\phi_{Al_2O_3} = 0.524$) cross-linking additions. $\phi_{Al_2O_3}$ for gelled samples was consistently higher than those without cross-linking agent additions. Recent work on the drying behavior of related bulk gelcast components[44] suggested that a contraction of the gel network during drying was responsible for the observed trends in particle-packing density.

(B) As-Cast Microstructures: SEM photomicrographs showing cross sections of as-cast bulk and SFF components cast from suspension containing [Ti] = 0.0 g of titanium/(mL of solution) and SFF-derived components cast at $R_{mix} = 5$ rpm and $R_{mix} = 300$ rpm from suspensions containing [Ti] = 6.30×10^{-3} g of titanium/(mL of solution) are shown in Figs. 10(a)–(d), respectively. A constant $d_t = 0.508$ mm was used for fabrication of these SFF samples. No microstructural differences were detected between bulk- and SFF-derived components, or SFF components formed in the absence of cross-linking agent additions. In all cases, particle packing was fairly uniform with no observable mixing rate effects. These results are reasonably consistent with measured ϕ_{solids} data described in the previous section, because only minimal variations in ϕ_{solids} with composition and R_{mix} were observed for these samples. No discernable microdefects (i.e., bubbles or cracking) were observed in either bulk- or SFF-derived components.

(C) Layer and Wall Uniformity: Optical microscopy and SEM images of a representative free-formed component cast at $R_{mix} = 100$ rpm and $d_t = 0.33$ mm from a suspension ($\phi_{Al_2O_3} = 0.45$, $\phi_{PVA}^{soln} = 0.05$) containing [Ti] = 3.041×10^{-3} g of titanium/(mL of solution) are shown in Figs. 11(a)–(d). Uniform layer thickness was observed, where the average individual layer thickness measured 0.20 ± 0.02 mm. Typical as-cast components had aspect ratios >7 and exhibited very little slumping, as demonstrated by the excellent wall uniformity illustrated in Fig. 11(c). Overpumping occurred during cornering, resulting in widening of the component walls in these regions. Minimal staircasing effects were observed for average wall thicknesses of 0.43 ± 0.01 mm (refer to Fig. 11(d)).

IV. Summary

The effects of processing parameters and suspension chemorheology on the deposition behavior of SFF components derived from polymeric-based gelcasting suspensions were studied for the first time. This novel route combined the advantages associated with SFF fabrication, including the ability to spatially tailor composition and structure as well as reduced tooling costs, with the improved handling strength afforded by the use of gel-based formulations. The shear rate profiles experienced during free-forming were estimated, and feedstock suspensions could be continuously printed for tip diameters ranging from 0.254 to 1.370 mm for all mixing rates and compositions studied. Line dimensions were independent of mixing rate for these process conditions. The as-cast alumina volume fraction depended on casting conditions and cross-linking agent concentration, where alumina volume

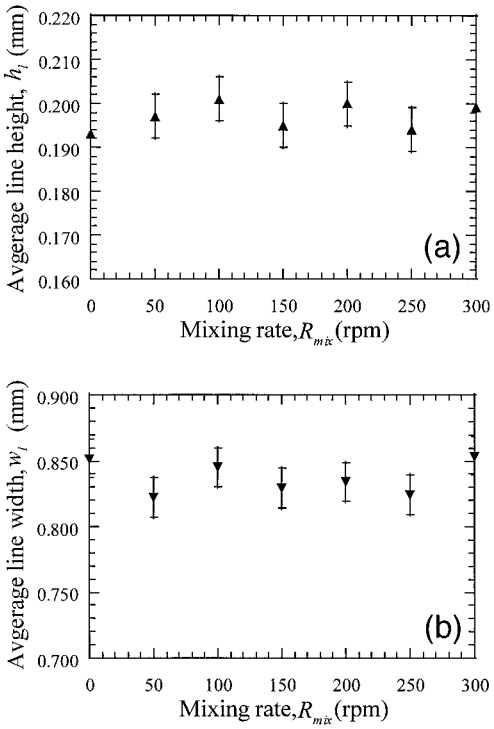

Fig. 8. Average line (a) height (h_l) and (b) width (w_l) as a function of mixing rate for dried lines cast from feedstock suspensions with $\phi_{Al_2O_3} = 0.45$, $\phi_{PVA} = 0.275$, and [Ti] = 3.041×10^{-3} g of titanium/(mL of solution) at varying mixing rates.

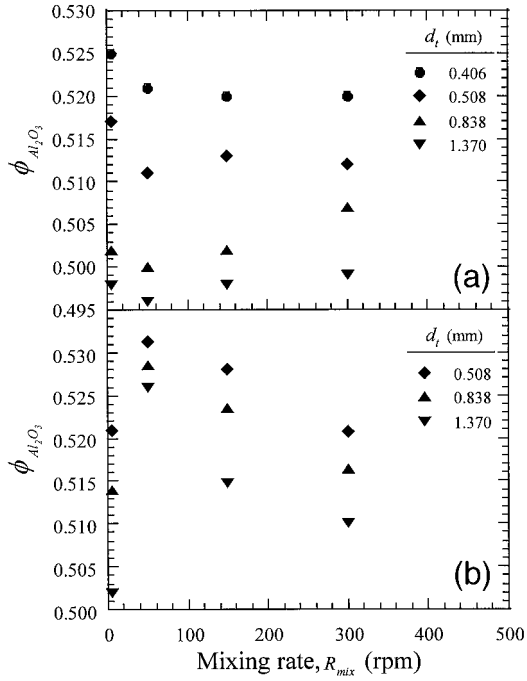

Fig. 9. Solids volume fraction ($\phi_{Al_2O_3}$) as a function of mixing rate (R_{mix}) and tip diameter (d_t) for as-cast components fabricated from suspensions ($\phi_{Al_2O_3} = 0.45$, $\phi_{PVA} = 0.5$) with varying cross-linking agent concentration ([Ti]): (a) 0 and (b) 6.30×10^{-3} g of titanium/(mL of solution).

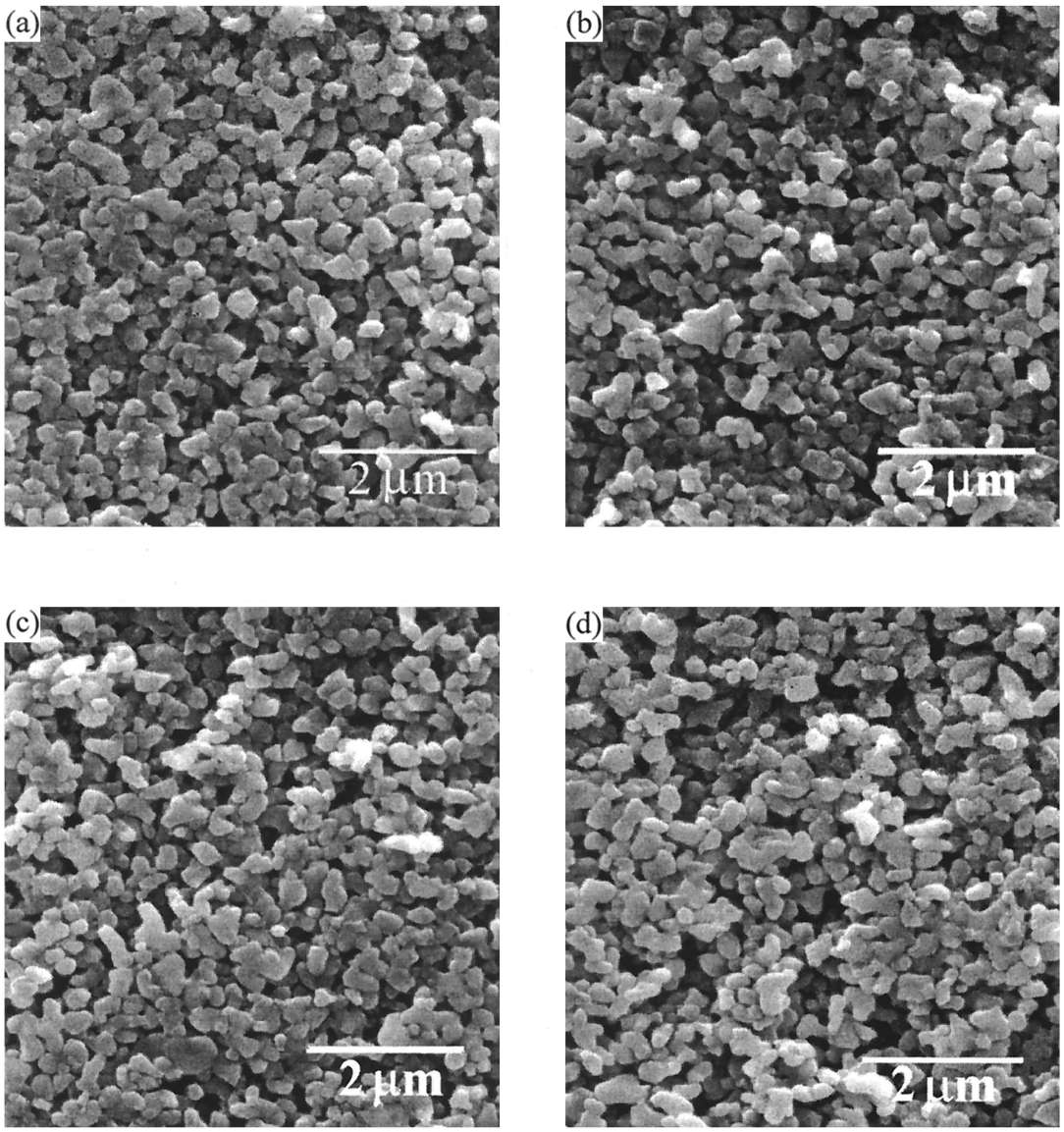

Fig. 10. SEM photomicrographs of as-cast (a) bulk and (b) SFF components cast from suspension containing 0.0 g of titanium/(mL of solution) and SFF-derived components cast at mixing rates of (c) 5 and (d) 300 rpm from suspensions containing 6.30×10^{-3} g of titanium/(mL of solution) (constant tip diameter of 0.508 mm was used for fabrication of SFF samples).

fraction increased with decreased tip diameter and increased cross-linking agent concentration. As-cast, free-formed alumina components exhibited uniform particle packing and had minimal macrodefects (e.g., slumping or staircasing) and no discernable microdefects (e.g., bubbles or cracking).

References

[1]M. Griffith and J. Halloran, "Ultraviolet Curable Ceramic Suspensions for Stereolithography of Ceramics"; presented at the ASME 1994 International Mechanical Engineering Congress and Exposition (Chicago, IL, 1994).

[2]M. Griffith and J. Halloran, "Stereolithography of Ceramics"; presented at the SAMPE 27th International Technical Conference (Albuquerque, NM, 1995).

[3]M. L. Griffith and J. W. Halloran, "Freeform Fabrication of Ceramics via Stereolithography," *J. Am. Ceram. Soc.*, **79** [10] 2601–608 (1996).

[4]C. Hinczewski, S. Corbel, and T. Chartier, "Stereolithography for Fabrication of Ceramic Three-Dimensional Parts," *Rapid Prototyping Journal*, **4** [3] 104–11 (1998).

[5]W. Cheng, J. Fuh, A. Nee, *et al*., "Multi-objective Optimization of Building Orientation in Stereolithography," *Rapid Prototyping Journal*, **1** [4] 12–23 (1995).

[6]G. Brady and J. Halloran, "Stereolithography of Ceramic Suspensions," *Rapid Prototyping Journal*, **3** [2] 61–65 (1997).

[7]M. Agarwala, V. Jamalabad, N. Langrana, *et al*., "Structural Quality of Parts Processed by Fused Deposition," *Rapid Prototyping Journal*, **2** [4] 4–19 (1996).

[8]M. Agarwala, A. Bandyopadhyay, R. van Weerwn, *et al*., "FDC, Rapid Fabrication of Structural Components," *Am. Ceram. Soc. Bull.*, **75** [11] 60–66 (1996).

[9]A. Bandyopadhyay, R. K. Panda, V. F. Janas, *et al*., "Processing of Piezocomposites by Fused Deposition Technique," *J. Am. Ceram. Soc.*, **80** [6] 1366–72 (1997).

[10]T. McNulty, F. Mohammadi, A. Bandyopadhyay, *et al*., "Development of a Binder Formulation for Fused Deposition of Ceramics," *Rapid Prototyping Journal*, **4** [4] 144–50 (1998).

[11]M. Yardimci, S. Guceri, and S. Danforth, "Process Modeling for Fused Deposition of Ceramics," *Ceram. Eng. Sci. Proc.*, **17** [3] 78–82 (1996).

[12]D. Klosterman, R. Chartoff, G. Graves, *et al*., "Direct Fabrication of Ceramics and Composites through Laminated Object Manufacturing (LOM)"; presented at the SAMPE International Symposium and Exhibition Proceedings (Covina, CA, 1998).

[13]J. Cawley, "Computer-Aided Manufacturing of Laminated Engineering Materials (CAM-LEM) and Its Applications to the Fabrication of Ceramic Components without Tooling"; pp. 1–5 in *Proceedings of the 1997 International Gas Turbine and Aeroengine Congress and Exposition*. ASME, New York, 1997.

[14]E. Sachs, M. Cima, D. Brancazio, *et al*., "Three-Dimensional Printing. Rapid Fabrication of Molds for Casting"; pp. 95–103 in *Advances in Integrated Product Design and Manufacturing*, Vol. 47. ASME, New York, 1991.

[15]E. Sachs, P. Williams, D. Brancazio, M. Cima, and K. Kremmin, "Three-Dimensional Printing. Rapid Tooling and Prototypes, Directly from a CAD Model," *Proc. Manuf. Int. '90*, **4**, 131–36 (1990).

[16]E. Sachs, M. Cima, and J. Bredt, "Three-Dimensional Printing of Ceramic Shells and Cores for Metal Casting," *Intelligent Design and Manufacturing for Prototyping, Am. Soc. Mech. Eng.*, [50] 61–72 (1991).

[17]E. Sachs, M. J.Cima, J. Cornie, *et al*., "Three-Dimensional Printing: The Physics and Implications of Additive Manufacturing," *Cirp Ann.*, **42** [1] 257–60 (1993).

[18]E. Sachs, M. Cima, P. Williams, *et al*., "Three-Dimensional Printing: Rapid Tooling and Prototypes Directly from CAD Model," *J. Eng. Ind.*, **114** [4] 481–88 (Nov. 1992).

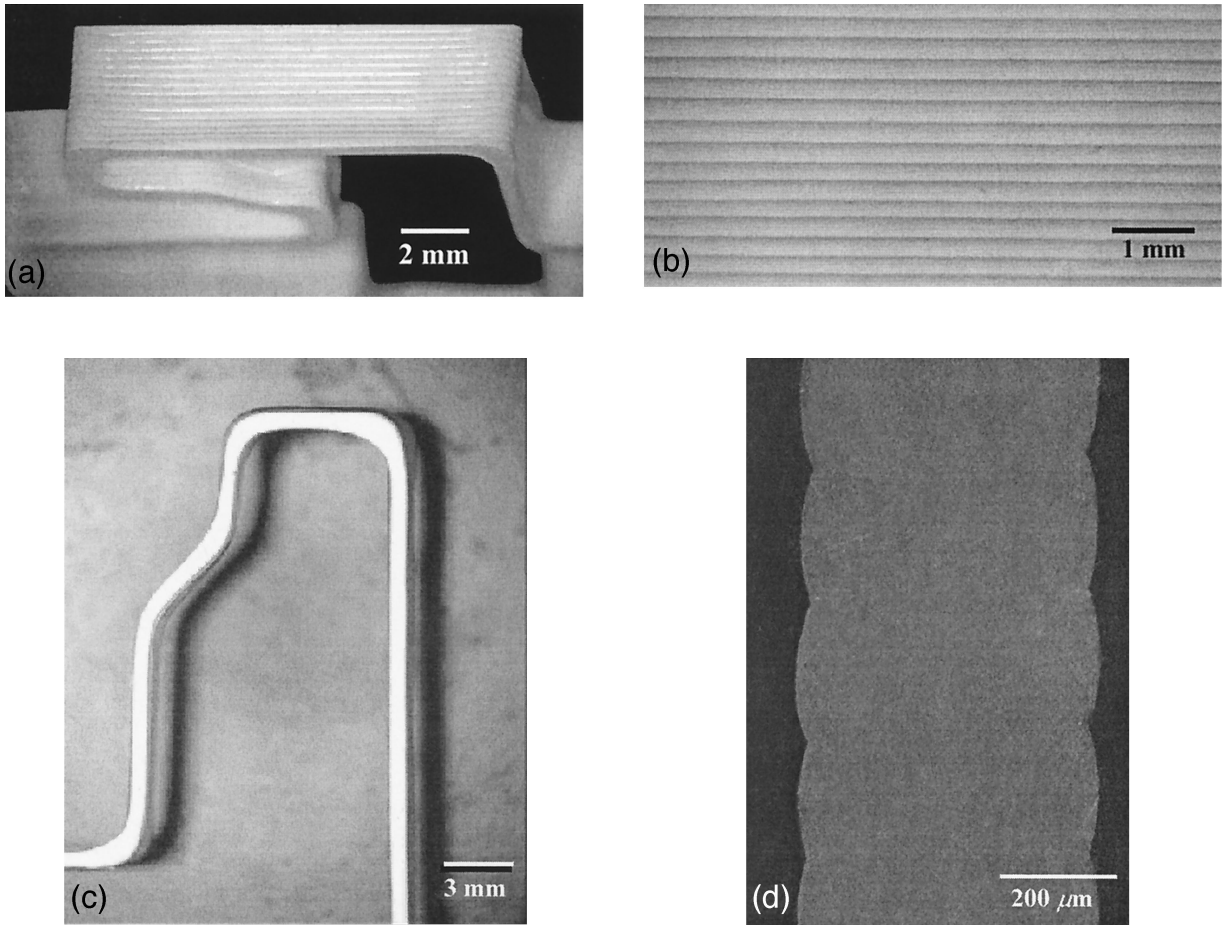

Fig. 11. Optical microscopy and SEM photomicrographs of a representative SFF-derived component showing (a) edge view, (b) close up view of edge section, (c) wall section, and (d) wall cross-section for a sample cast using a 0.330 mm tip at a mixing rate of 100 rpm from a feedstock suspension containing 3.041×10^{-3} g of titanium/(mL of solution).

[19]J. Cesarano III and T. A. Baer, "Recent Developments in Freeform Fabrication of Dense Ceramics from Slurry Deposition"; presented at the Solid Freeform Fabrication Symposium (University of Texas at Austin, Austin, TX, 1997).

[20]J. Cesarano III, B. King, and H. Denham, "Recent Developments in Robocasting of Ceramics and Multimaterial Deposition"; presented at the Solid Freeform Fabrication Symposium (University of Texas at Austin, Austin, TX, 1998).

[21]A. C. Young, O. O. Omatete, M. A. Janney, *et al*., "Gelcasting of Alumina," *J. Am. Ceram. Soc.*, **74** [3] 612–18 (1991).

[22]O. O. Omatete, R. A. Strehlow, and C. A. Walls, "Gelcasting of Submicron Alumina, SiAlON, and Silicon Nitride Powders"; presented at the 37th Sagamore Army Materials Research Conference (Plymouth, MA, 1990).

[23]O. O. Omatete, private communication, Nov. 1997.

[24]O. O. Omatete and A. Bleier, "Tailoring Suspension Flow for the Gelcasting of Oxide and Non-Oxide Ceramics," *Mater. Res. Soc. Symp. Proc.*, **346**, 357–63 (1994).

[25]O. O. Omatete, A. Bleier, C. G. Westmoreland, *et al*., "Gelcast Zirconia–Alumina Composites," *Ceram. Eng. Sci. Proc.*, **12** [9–10] 2084–94 (1991).

[26]O. O. Omatete, M. A. Janney, and R. A. Strehlow, "Gelcasting—A New Ceramic Forming Process," *Am. Ceram. Soc. Bull.*, **70** [10] 1641–49 (1991).

[27]S. L. Morissette and J. A. Lewis, "Chemorheology of Aqueous Alumina–Poly(vinyl alcohol). Gelcasting Suspensions," *J. Am. Ceram. Soc.*, **82** [3] 521–28 (1999).

[28]S. L. Morissette and J. A. Lewis, "Gelcasting of Al_2O_3–PVA Suspensions"; presented at the 98th Annual Meeting of the American Ceramic Society, Cincinnati, OH, May 2, 1995 (Science, Technology, and Commercialization of Powder Synthesis and Shape-Forming Processes Symposium, Poster No. SXIXP-17–95).

[29]M. Huha and J. A. Lewis, "Polymer Effects on the Chemorheological and Drying Behavior of Alumina–Poly(vinyl alcohol) Gelcasting Suspensions," *J. Am. Ceram. Soc.*, **83** [8] 1957–63 (2000).

[30]M. Huha and J. A. Lewis, "Influence of Defoamer Additions and Polymer Hydrolysis on the Properties of Alumina–PVA Gelcasting Systems"; pp. 141–50 in Ceramic Transactions, Vol. 108, *Innovative Processing and Synthesis of Ceramics, Glasses, and Composites III*. Edited by J. P. Singh, N. P. Bansel, and K. Niihara. American Ceramic Society, Westerville, OH, 1999.

[31]K. Stuffle, A. Mulligan, J. Lombardi, *et al*., "Solid Freebody Forming of Ceramics from Polymerizable Slurry"; pp. 1027–31 in *Better Ceramics through Chemistry*, Vol. VI, Materials Research Society Symposium Proceedings. Materials Research Society, Pittsburgh, PA, 1994.

[32]J. Lombardi, G. George, L. Rintoul, *et al*., "Freeform Fabrication of Polymers and Composites," *Polymer Preprints*, **37** [1] 221–22 (1996).

[33]S. L. Morissette, J. A. Lewis, J. Cesarano III, and D. B. Dimos, "Solid Freeform Fabrication Using Alumina–Poly(vinyl alcohol) Gel-Casting Suspensions"; pp. 125–30 in *Solid Freeform and Additive Fabrication*, Vol. 542, Materials Research Society Symposium Proceedings. Edited by D. Dimos, S. C. Danforth, and M. J. Cima. Materials Research Society, Pittsburgh, PA, 1998.

[34]Product literature, Darvan C (NC-94–06), R. T. Vanderbilt, Norwalk, CT, 1999.

[35]Product literature, 405S Poly(vinyl alcohol), Kuraray International, New York, 1997.

[36]P. G. Desai, J. A. Lewis, and D. P. Bentz, "Unreacted Cement Content in Macro-Defect-Free Composites—Impact on Processing Structure Property Relations," *J. Mater. Sci.*, **29** [24] 6445–52 (1994).

[37]M. Gülgün, O. Popoola, and W. Kriven, "X-ray Photoelectron Spectroscopy Studies of Bond Structure between Poly(vinyl alcohol) and a Titanate Cross-Coupling Agent," *J. Mater. Res.*, **10** [6] 1565–71 (1995).

[38]Product literature, Tyzor TE, DuPont Chemicals, Deepwater, NJ, 1998.

[39]R. C. East, M. J. Astyl, and W. H. Beyer, *Handbook of Chemistry and Physics*; p. F125. CRC Press, Boca Raton, FL, 1985.

[40]W. S. Janna, *Introduction to Fluid Mechanics*; p. 232. PWS-Kent, Boston, MA, 1993.

[41]J. E. Sergent and C. A. Harper, *Hybrid Microelectronics Handbook*. McGraw-Hill, New York, 1995.

[42]J. A. Reed, *Introduction to the Principles of Ceramic Processing*. Wiley-Interscience, New York, 1988.

[43]P. R. Schunk, P. A. Sackinger, R. R. Rao, *et al*., "GOMA 2.0–A Full-Newton Finite-Element Program for Free- and Moving-Boundary Problems with Coupled Fluid/Solid Momentum, Energy, Mass, and Chemistry. Species Transport: User's Guide," Tech. Rept. SAND97–2404. Edited by Sandia National Laboratories. Sandia National Laboratories, Albuquerque, NM, 1997.

[44]S. Ghosal and A. Emami Naeini, "A Physical Model for the Drying of Gelcast Ceramics," *J. Am. Ceram. Soc.*, **82** [3] 513–20 (1999). □